

1 ASEP with periodic boundary conditions

A discussion of the space-time diagrams can be seen in figure 4d and 5d.

Figures 1 and 2 show the fundamental diagram of the ASEP with periodic boundary conditions for $q = 0.5$ and $q = 0.7$. In each case, only the random sequential update method coincides with the mean-field prediction $J(\rho) = q\rho(1 - \rho)$. All other update methods deliver consistently greater fluxes for a specific density. By comparing $q = 0.5$ to $q = 0.7$, one can see that a higher q increases the flux J . An exemplary proof of convergence is included in figure 3, where a fast convergence to the steady state can be seen.

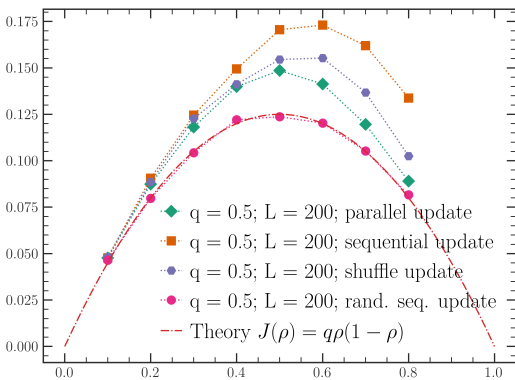


Figure 1: Fundamental diagram of the ASEP with $q = 0.5$ simulated using the different update methods.

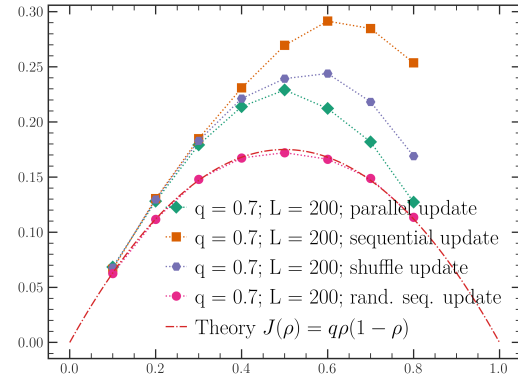


Figure 2: Fundamental diagram of the ASEP with $q = 0.7$ simulated using the different update methods.

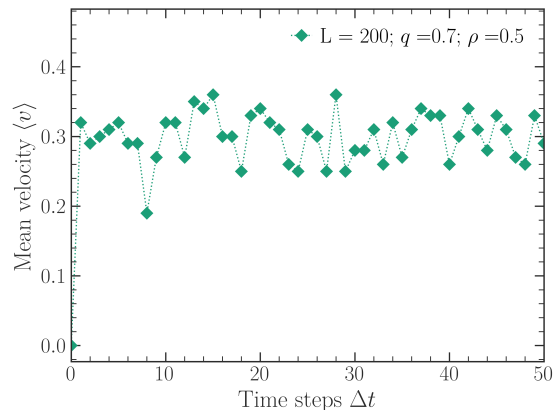
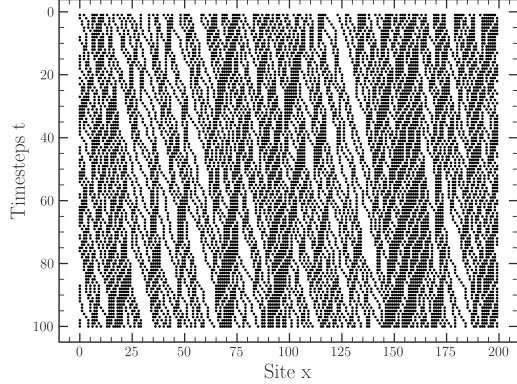
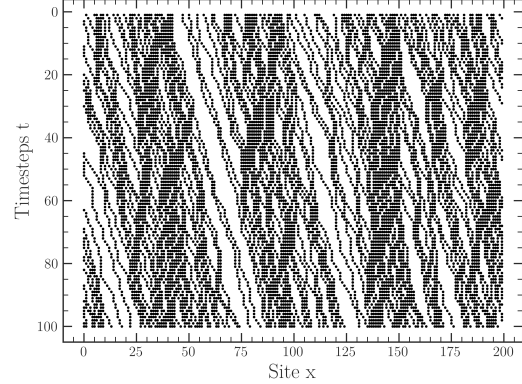


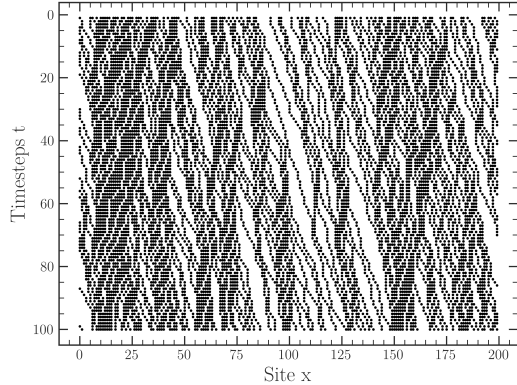
Figure 3: Exemplary plot to show the convergence of the mean velocity $\langle v \rangle$ with $q = 0.7$ and $\rho = 0.5$. As an update method, the random sequential update was used.



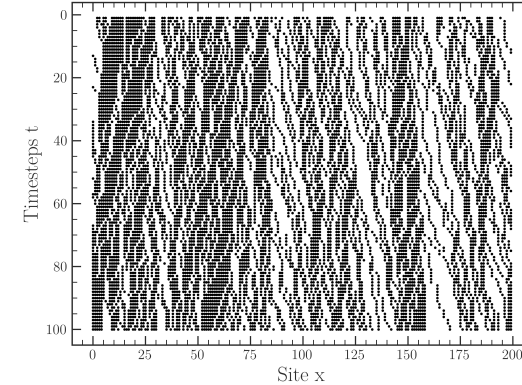
(a) ASEP with $q = 0.5$, $\rho = 0.5$ with parallel updates.
Last 100 steps of the simulation.



(b) ASEP with $q = 0.5$, $\rho = 0.5$ with sequential updates.
Last 100 steps of the simulation.

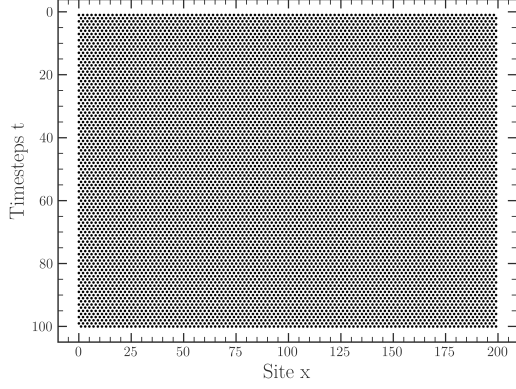


(c) ASEP with $q = 0.5$, $\rho = 0.5$ with shuffle updates.
Last 100 steps of the simulation.

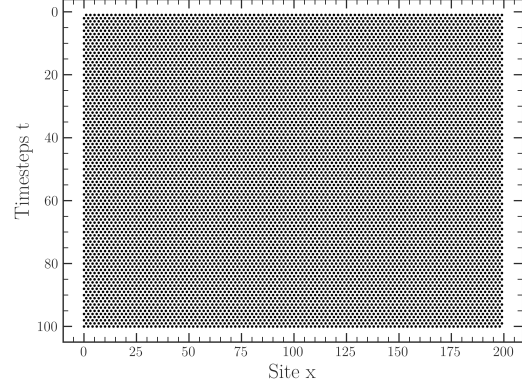


(d) ASEP with $q = 0.5$, $\rho = 0.5$ with random sequential updates. Last 100 steps of the simulation.

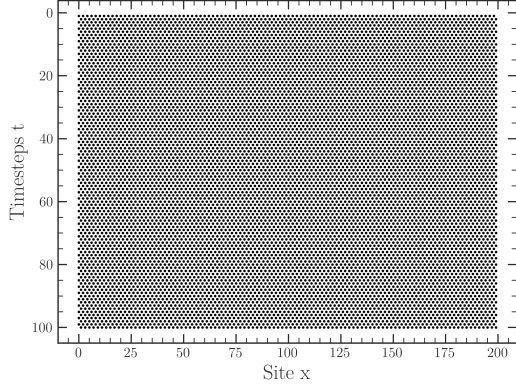
Figure 4: Simulation of the asymmetric simple exclusion process for $q = 0.5$ and $\rho = 0.5$ for the four different update methods. The spontaneous formation can be observed for all update methods. There is no clear difference in the likelihood of the occurrences of such jams.



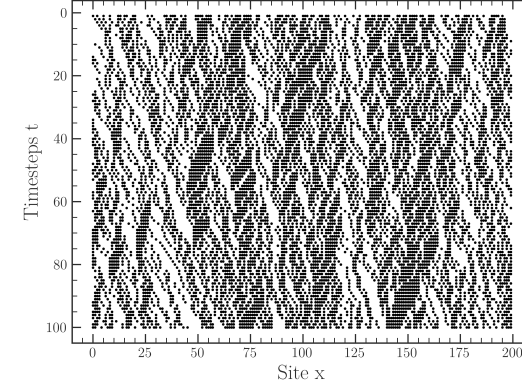
(a) ASEP with $q = 1$, $\rho = 0.5$ with parallel updates.
Last 100 steps of the simulation.



(b) ASEP with $q = 1$, $\rho = 0.5$ with sequential updates.
Last 100 steps of the simulation.



(c) ASEP with $q = 1$, $\rho = 0.5$ with shuffle updates. Last
100 steps of the simulation.



(d) ASEP with $q = 1$, $\rho = 0.5$ with random sequential
updates. Last 100 steps of the simulation.

Figure 5: Simulation of the asymmetric simple exclusion process for $q = 1$ and $\rho = 0.5$ for the four different update methods. For this specific case, there is a clear distinction between the random sequential updates and the other three methods. Remember, that the last 100 steps of the simulation are plotted. Since in the update methods a) - c), we move every particle with certainty in a single update step, we eventually reach a steady state, where each particle moves freely. This event is also only possible for $\rho \leq 0.5$. With random sequential updates, it is not guaranteed that we move every particle during an update steps. Therefore, that steady state can not develop.

2 ASEP with open boundary conditions

The low density phase (A) is shown in figures 7 and 8, where $\rho < 0.5$. Figures 9 and 10 are illustrating the high density phase (B), where $\rho > 0.5$. Figure 11 shows the high-current phase (C), where the density is $\rho \approx 0.5$ and shows a peak at the first sites and a decay of the density at the last sites.

Figure 12 shows the averaged density of the ASEP with open boundary conditions for different values of α and β (still $q = 0.8$). The geometry of the phase transition can clearly be seen. The high current phase, where $\rho \approx 0.5$, also appears quite clearly. Additionally, it can be spotted that there has to be a phase transition for $\alpha = \beta$. The same thing is true for figure 13: the high current phase can be spotted even more easily.

In order to distinguish the different sub-phases in the low-density and high-density phase, a scalar quantity had to be constructed. A first try with using the gradient of the density profile yielded no good result. Then, we relapsed back to a more simple expression $\Delta\rho = \rho[-1] - \rho[0]$, where we compare the density of the last site to the first. The phase transition is then characterized by $\Delta\rho = 0$. Figure 14 shows the shape parameter $\Delta\rho$ for different α and β . The phase transition dividing A and dividing B should be given by $\Delta\rho = 0$. Therefore, we observe that the phase transition does not have the circular shape of the analytical approach, but has more of a linear character.

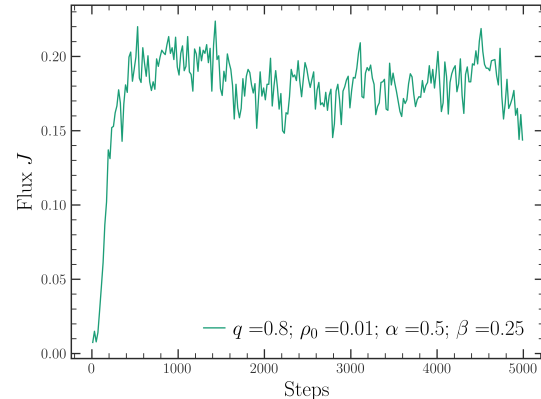


Figure 6: Exemplary illustration of convergence of the flux with $q = 0.8$, $\alpha = 0.5$ and $\beta = 0.25$. The starting density of the simulation was chosen to be $\rho_0 = 0.01$.

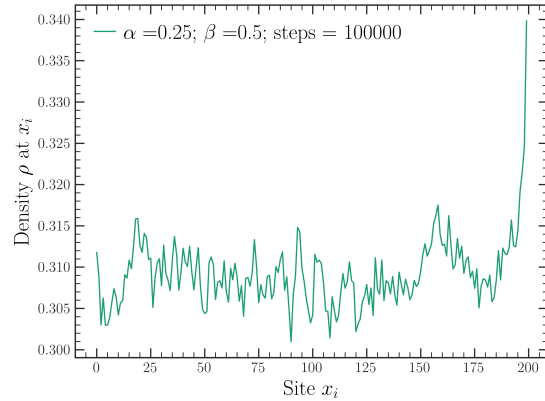


Figure 7: Density profile $\rho(x_i)$ of the ASEP with open boundary conditions, where $q = 0.8$, $\alpha = 0.25$ and $\beta = 0.5$.

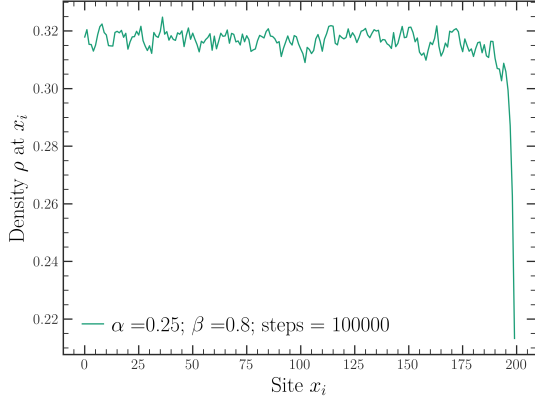


Figure 8: Density profile $\rho(x_i)$ of the ASEP with open boundary conditions, where $q = 0.8$, $\alpha = 0.25$ and $\beta = 0.8$.

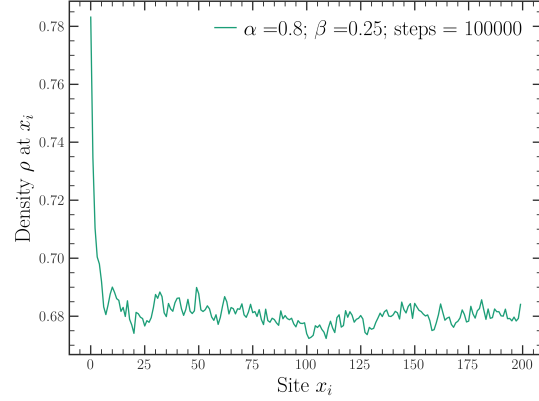


Figure 10: Density profile $\rho(x_i)$ of the ASEP with open boundary conditions, where $q = 0.8$, $\alpha = 0.8$ and $\beta = 0.25$.

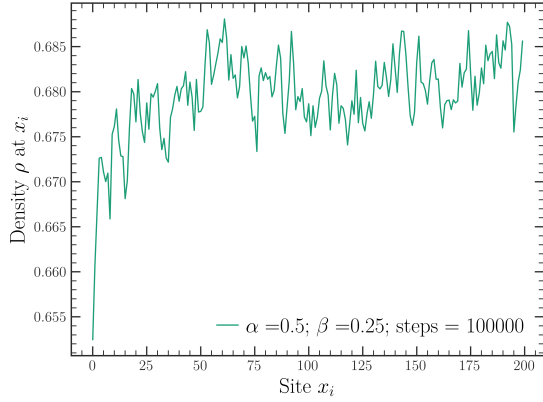


Figure 9: Density profile $\rho(x_i)$ of the ASEP with open boundary conditions, where $q = 0.8$, $\alpha = 0.5$ and $\beta = 0.25$.

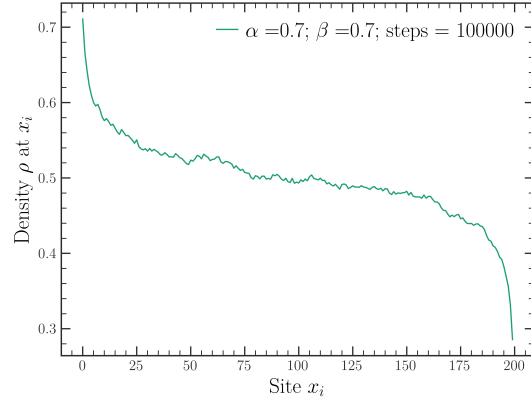


Figure 11: Density profile $\rho(x_i)$ of the ASEP with open boundary conditions, where $q = 0.8$, $\alpha = 0.7$ and $\beta = 0.7$.

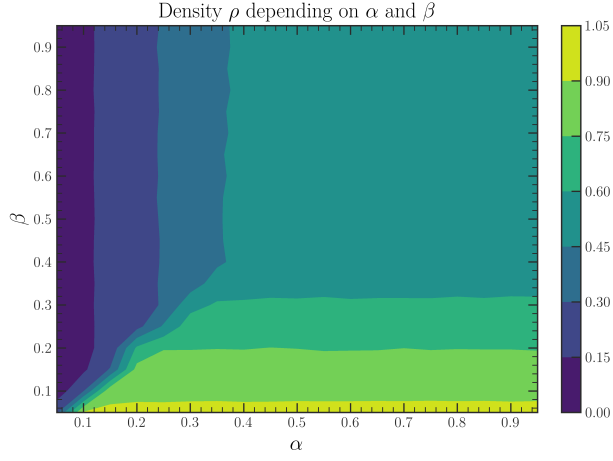


Figure 12: Density of the ASEP with open boundary conditions with $q = 0.8$ for different values of α and β .

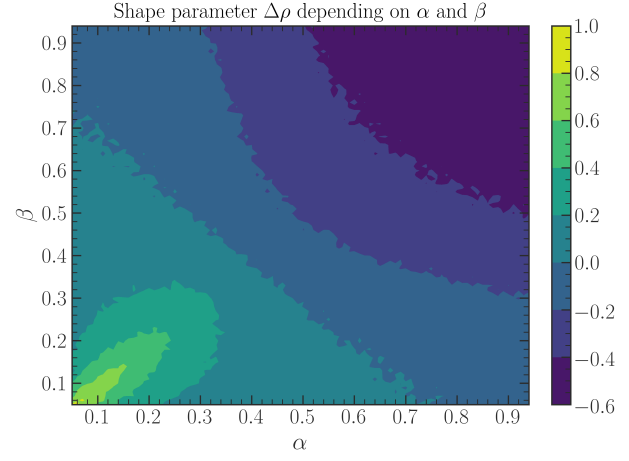


Figure 14: Shape parameter $\Delta\rho$ of the density profiles with $q = 0.8$ for different values of α and β . A phase transition can be observed at $\Delta\rho = 0$.

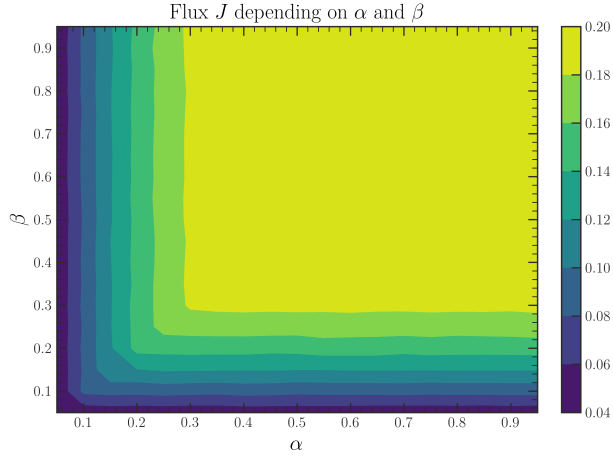


Figure 13: Flux J of the ASEP with open boundary conditions with $q = 0.8$ for different values of α and β .

3 Nagel-Schreckenberg model

Figures 15, 16 and 17 show some exemplary space-time diagrams for the Nagel-Schreckenberg model. In all three figures, the spontaneous formation of jams can be observed. By comparing the plots to the ASEP, the effect of acceleration and deceleration can clearly be seen. Qualitatively, the diagram is divided into jams and free flow phases. The agents are able to accelerate in free flow phases, while the jams lead to deceleration. By varying ρ , one is able to increase the occurrences of jams. By changing p , one can influence the velocity of a jam travelling backwards. To translate the velocity of the traffic jam from our simulation to the real world, we have to define the site spacing and the time step in real space distances and time intervals. We take the distance between different sites to be $\Delta x = 5$ m. Furthermore, we assume $v_{\max} = 130$ km/h. This automatically fixes the time step to $\Delta t = \frac{5 \text{ m}}{3.61 \text{ m/s}} \approx 1.4$ s. With these constants, the velocity of the jams in figure 15 can be calculated to be 10.30 km/h. The other velocities evaluate to 10.28 km/h (fig 16) and 5.8 km/h (fig. 17).

In order to estimate the p value corresponding to a realistic velocity of a traffic jam of 15 km/h, we have to look at the first car defining the start of the traffic jam. With probability p . the car does not accelerate. The average velocity of the first car is therefore $\langle v \rangle = v(1 - p)$, where v is the velocity of a car accelerating. When we take $v = 20$ km/h, we obtain $p = 0.25$. Therefore, $p < 0.25$ correspond to the realistic scenario.

Figure 18 shows the fundamental diagram of the Nagel-Schreckenberg model. As expected, one can observe *free flow* states and the *congested* states, as well as a metastable branch. Additionally, one can see that the flux in the free flow states is independent of p . However, the flux in the congested states shows a strong dependence on p , which makes total sense since a larger p leads to more "interaction". Figure 19 illustrates that the mean velocity and therefore

the flux converges nicely.

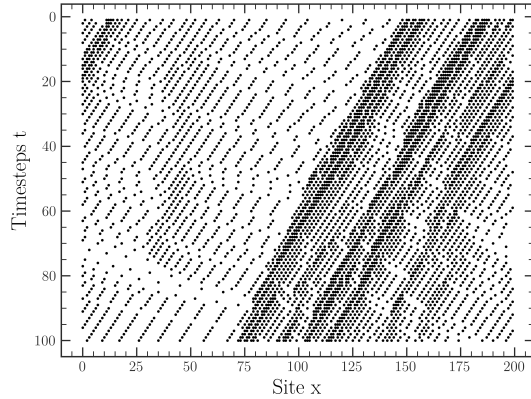


Figure 15: Space-time diagram for the Nagel-Schreckenberg model with $\rho = 0.25$ and $p = 0.1$. Spontaneous formations of jams can be noticed.

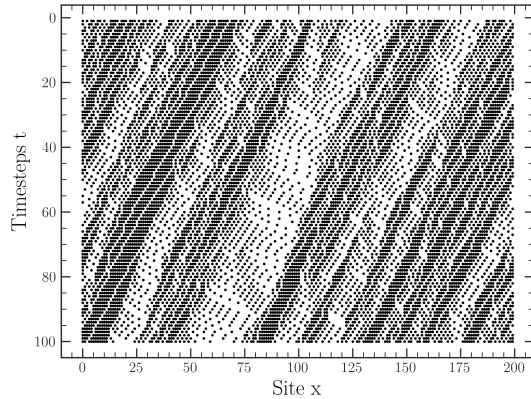


Figure 16: Space-time diagram for the Nagel-Schreckenberg model with $\rho = 0.5$ and $p = 0.2$. Spontaneous formations of jams can be noticed.

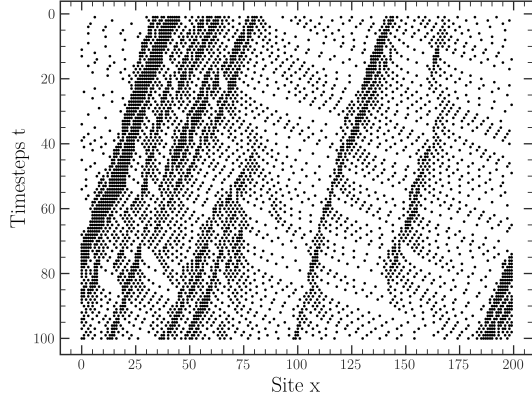


Figure 17: Space-time diagram for the Nagel-Schreckenberg model with $\rho = 0.25$ and $p = 0.3$. Spontaneous formations of jams can be noticed.

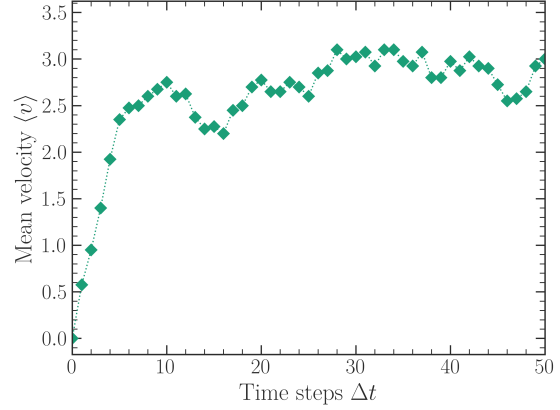


Figure 19: Exemplary illustration of convergence of the mean velocity with $p = 0.2$ and $\rho = 0.2$.

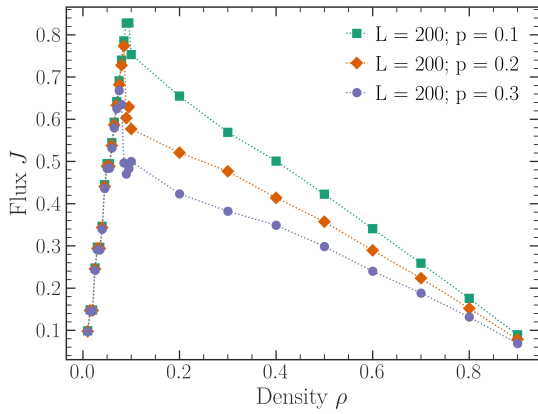


Figure 18: Fundamental diagram of the Nagel-Schreckenberg model with $p = 0.2$ and $L = 200$. The *free flow* states and the *congested* states can be seen clearly. Even the metastable branch can be observed.

4 Velocity-Dependent Randomization model

Some exemplary space-time diagrams of the VDR model are illustrated in figures 20, 21 and 22. For large differences between p and p_0 , there is the tendency that the width of traffic jams is increased considerable. For smaller differences, like in figure 21, the difference to the Nagel-Schreckenberg model can hardly be noticed.

Figure 23 shows the fundamental diagram of the VDR model. It exhibits the same features as the fundamental diagram of the Nagel-Schreckenberg model. However, since the interaction was increased with p_0 , the congested states show a much lower flux than before. It is also noteworthy, that the fundamental diagram does not depend that strongly on p anymore. From that we can conclude, that much of the interaction behavior is actually encoded in p_0 . Figure 24 shows how the mean velocity converges nicely.

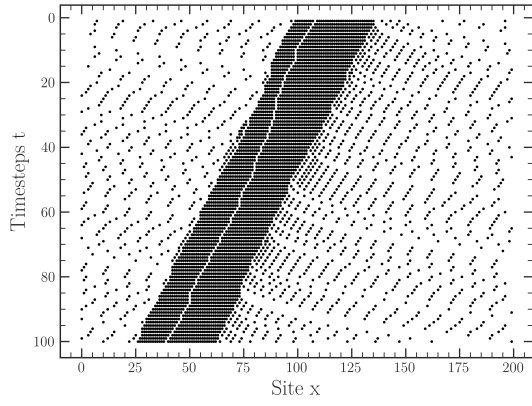


Figure 20: Space-time diagram the VDR model with $\rho = 0.25$, $p = 0.1$ and $p_0 = 0.3$.

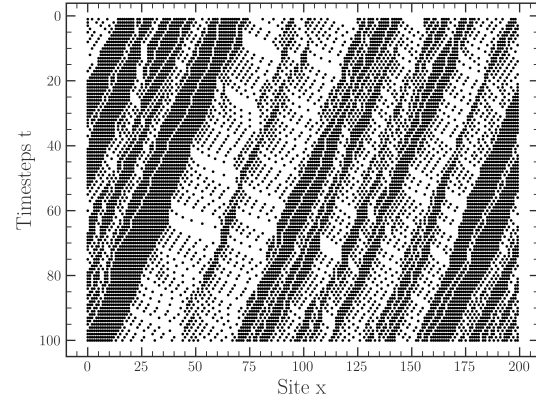


Figure 21: Space-time diagram for the VDR model with $\rho = 0.5$, $p = 0.2$ and $p_0 = 0.3$.

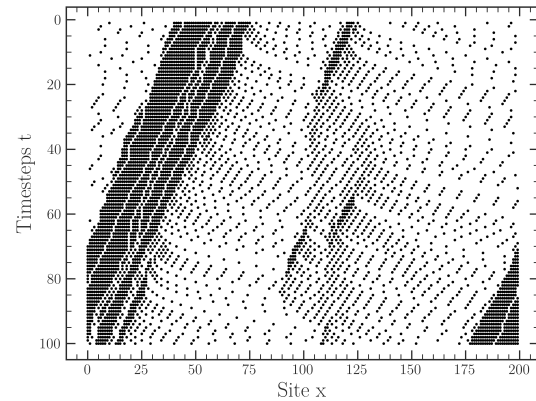


Figure 22: Space-time diagram for the VDR model with $\rho = 0.25$, $p = 0.15$ and $p_0 = 0.3$.

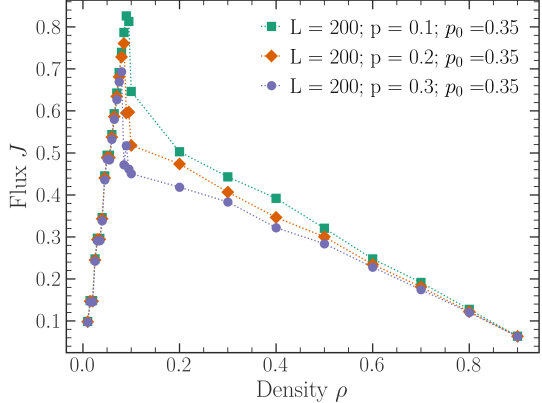


Figure 23: Fundamental diagram of the VDR model with $p = 0.2$, $p_0 = 0.35$ and $L = 200$. The *free flow* states and the *congested* states can be seen clearly.

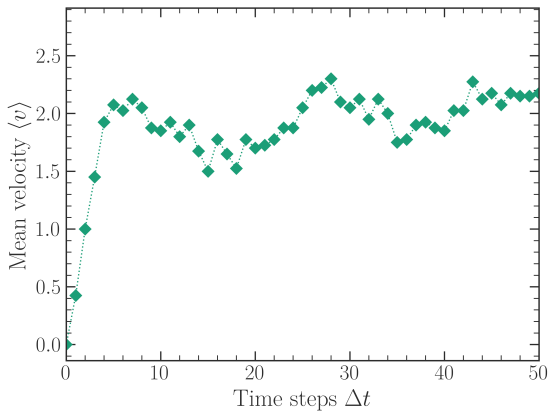


Figure 24: Exemplary illustration of convergence of the mean velocity with $p = 0.2$, $p_0 = 0.35$ and $\rho = 0.2$.